Photoluminescence behaviour of erbium implanted in sodium containing silicate glasses

P.G. Kik
Supervisors: Drs. E. Snoeks and Dr. A. Polman

Abstract

Erbium was implanted in 2 mm thick BGG31, a new sodium containing silica glass designed for the fabrication of optical waveguides, at fluences ranging from $0.9 \cdot 10^{15}$ Er/cm^2 to $1.2 \cdot 10^{16}$ Er/cm^2, corresponding to 0.1 at.% and 1.7 at.% respectively. When pumped at 488 nm the samples showed typical Er^{3+} photoluminescence (PL), with maximum luminescence intensity at 1532 nm. Annealing at temperatures ranging from 300°C to 570°C resulted in an increase of the PL intensity. The decay characteristics of the luminescent state were measured, showing non exponential decay for annealing temperatures below 400°C. This is attributed to non radiative energy transfer from the Er excited state to implantation induced defects. Above 400°C annealing lifetimes of the order of 1 ms were observed. The PL intensity is found to increase sublinearly with fluence. This behaviour is explained in terms of a measured increase in the non radiative decay rate as function of fluence due to Er-Er and Er-defect interactions. Pump power dependent measurements of the PL intensity and PL lifetime yielded an upper limit for the absorption cross-section at 488 nm of $5.4 \cdot 10^{-21}$ cm^2 ± 30%. Furthermore these measurements showed that for pump intensities of the order of 10 kW cm^{-2} possibly processes such as upconversion play a role. A positive correlation is found between OH content and PL decay rate in BGG31 glass, soda-lime glass, tempax glass, Corning 0211 glass, Pilkington soda-lime glass and witglas. This is attributed to a resonance between the Er^{3+} transition and an overtone of the OH stretch vibration.

Contents

1. INTRODUCTION

1.1 Motivation

The experiments described in this report are part of a large research program on integrated optics. The goal of these particular experiments was to examine the applicability of the rare earth Er as light amplifier in a new glass type. Light amplifiers are needed in the field of optical data transmission and integrated optics, fields that will probably continue their fast growth for many years. Light amplifiers can compensate for signal loss during transport, and thus open the road to long range optical data transmission with its enormous transport capacity.

1.2 Telecommunication and integrated optics

In the field of telecommunication the use of glass fiber for data transmission is becoming more and more important. Because of the high frequency of light, optical signals sent through fibers can be modulated over an enormous bandwidth. Different wavelengths can travel along the same fiber without interfering, offering further transport capacity. Moreover, optical signals can travel around the world in two tenths of a second. With the combined use of these three features, error-free data transmission rates of 10 Gbit/s have been achieved[1] over a distance of one million kilometres. This was done in a fiber loop, using an Er based light amplifier.

The use of fiber technology in telecommunication asks for switching- and multiplexing devices comparable to those used in electronic telecommunication. The design and integration of these types of components is done in the field of integrated optics. In this field optical amplifiers are needed to compensate for intrinsic intensity loss in the guiding material and for the intensity drop after splitting of signals. A beam splitter for example requires 3 dB amplification in both output channels, while the best optical amplifiers in integrated optics reach 3.3 dB/cm gain[2]. Much work is done to enhance the efficiency of these amplifiers.

The structures that form the basis for optical components are planar optical waveguides. Optical waveguides are structures that can guide light by means of total internal reflection. This light confinement can be achieved by giving part of the transparent waveguide material a slightly higher index of refraction than its surroundings, and inserting light with a very narrow angular spread. The optical properties of planar waveguides can be adjusted locally by doping with various materials, which is a very attractive feature for integration of optical components.

Ion exchange represents a common way to fabricate planar waveguides. With this technique the index change is brought about by exchanging a specific ion type in the waveguide material for index raising ions. The exchange is accomplished using an ion diffusion process. For sodium containing glasses usually the $Na^+ \leftrightarrow K^+$ ion exchange is applied. Because of the relatively low index change per K^+ ion, this requires rather broad index profiles with typical depths of 5 µm.[3] This size is similar to the width of light propagation modes inside optical fibers, allowing for low-loss coupling of fibers to planar waveguides. Typical losses in potassium exchanged waveguides however are still of the order of 0.8 dB/cm, which is very high compared to the typical 1 dB/km losses inside fibers. To improve the transmission characteristics, new glasses are designed especially for waveguide formation.

1.3 Some erbium characteristics

The rare earth metal erbium, discovered in 1842 in a Swedish town called Ytterby, is one of the few materials that are used for light amplification in telecommunication. The main advantage of Er is that the Er^{3+} ion exhibits an optical transition at 1.5 µm, which coincides with the optical window - the wavelength region with the least attenuation - of most commercially available fibers and glasses. It is one of the standard communication wavelengths in present telecommunication.

In the periodic system Er can be found among the Lanthanides, a group of elements with very similar chemical properties. This chemical similarity is due to the fact that all these elements have the same outer electron shell configuration ($5s^2 5p^6 6s^2$). While the outer shell configuration remains the same, the occupancy of one of the inner shells, the 4f shell, is increasing along the Lanthanides. In the Er^{3+} ion, eleven of the available fourteen electron states in the 4f shell are occupied. This leaves a degree of freedom to the spin configuration in this level, giving different energy levels. As a result several intra 4f transitions are possible (fig. 1). The 1.5 µm transition used for light amplification is the transition from the $^4I_{13/2}$ to the $^4I_{15/2}$ state.

All the intra 4f configurations in the free Er^{3+} ion have the same 4f-like orbit. The emission or absorption of a photon however requires a radical change in the symmetry, namely a change in parity, of the 4f wave functions. The consequence of this is that optical intra 4f transitions are parity forbidden. They can only occur when the symmetry of the 4f electron wave functions is distorted to a certain degree.

When erbium is ionically bound inside a certain host material, the electric fields from the surrounding nuclei influence the 4f wave functions, allowing optical intra 4f transitions to occur. The distortion however is moderated by the presence of the outer electron shells, resulting in similar optical properties inside many different materials.

1.4 Advantages of Er in light amplifiers

There are several aspects that make the Er ion such an interesting candidate for optical amplifiers. The main reason to choose erbium lies in the fact that the 1.5 µm light emitted by one of the intra 4f transitions turns out to be in the optical window, and coincides with a standard telecommunication wavelength.

Another important reason to choose Er is the extremely long decay lifetime of the 1.5 µm level. Once an Er ion is in the 1.5 µm excited state, it can stay there for several milliseconds, depending on host material. This is due to the fact that the optical transition is parity forbidden, combined with the fact that the energy difference with the ground state is large compared to typical phonon energies. Due to the described shielding effect of the outer electron shells Er shows long lifetime 1.5 µm states in many host materials. Because of the long lifetime it is easy to reach the population inversion needed for amplification.

A very crucial feature of the Er level system is the fact that the 1.5 µm level can be pumped via higher excited states. These states rapidly decay into the 1.5 µm level by means of a multiphonon relaxation process. This makes it possible to exclude stimulated emission by the pump laser, allowing population inversion to be higher than fifty percent. Another way of avoiding part of the stimulated emission is

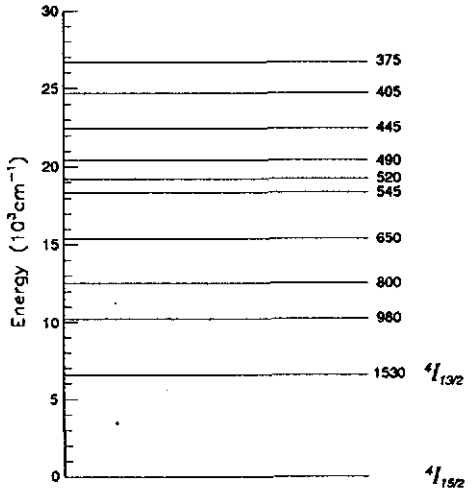

fig 1: free Er^{3+} emission lines with their emission wavelengths (nm)

pumping in the high energy side of the broad 1.5 μm level. The excited state preferentially resides at the low energy side of the level, thereby decreasing the overlap of the pump light with the excited state.

A last favourable aspect is the spectral width of the 1.5 μm transition. Widths of 80 nm have been observed,[4] enabling amplification over the corresponding frequency range. This allows for wavelength divisioning of the optical signal, increasing the transport capacity. The broadness of the spectrum is caused by the host material, as will be explained in more detail in section 3.4.2.

2. EXPERIMENTAL TECHNIQUES

2.1 Implantation

In the process of ion implantation ions are incorporated in the host material by shooting them into the sample. Having entered the sample, the ions are slowed down by electronic excitations and collisions with nuclei. This method of course results in a damaged material structure, but often the structural damage can be undone after the implantation. Besides this, ion implantation has a number of important advantages. Implantation is a non-equilibrium technique, so the resulting composition is not subject to the laws of thermodynamics. In principle it is possible to dope any material up to any concentration without precipitation. This means that for example optical doping can be achieved easily, regardless of material composition. The concentration profile that is the result of the stochastic stopping process has a Gaussian shape, which matches the light intensity distribution inside waveguides quite well. Furthermore the depth of the profile can be controlled freely by varying the energy of the incoming ions.

Implantations are commonly performed with a van de Graaff type accelerator (fig 2). In this type of accelerator the terminal voltage is created by means of a rapidly moving belt that transports charge from ground potential to the high voltage terminal shell. With the implantation system at AMOLF a terminal voltage of 1 MV can be reached. To shield the terminal shell from ground voltage, the shell is encapsulated in a pressure vessel, containing a mixture of insulating SF_6 gas with N_2 at a pressure of 5 bar. The high energy ions leaving the pressure vessel are deflected in a mass selection magnet, to prevent coimplantation of other elements present in the ion source. A homogeneous implantation is acquired by scanning the beam electrostatically across the sample.

2.2 Rutherford Backscattering Spectrometry

In Rutherford Backscattering Spectrometry (RBS) high energy ions are used to determine material composition as a function of depth. The setup is similar to that in figure 2, with the addition of an energy sensitive particle detector in the sample chamber. During an RBS measurement the energy of the particles backscattered from the samples is measured. In practice all of the observed scattering events are two particle collisions. This means that the kinetic energy of an ion scattered from an atom at the sample surface is determined by the laws of classical mechanics, and for a given angle contains only the mass of the target atom as unknown variable. As heavy atoms in the sample will hardly pick up energy from the light probing ion (^{4}He in these experiments), ions scattered from different heavy elements will have similar energies. This results in a decrease in resolution for the heavy elements.

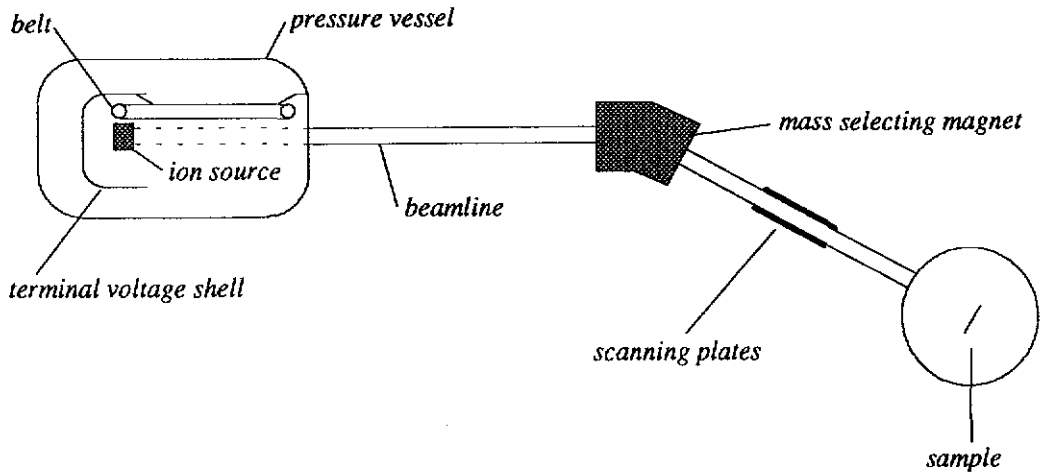

fig 2 :Schematic picture of a van de Graaff type accelerator, used for implantation

The depth resolution is obtained by evaluating the electronic stopping in the sample. Ions penetrating the sample are slowed down, and will have a lower energy when backscattered than ions scattered from the surface. This effect extends the signal from one specific element over a whole range of energies. Thus with knowledge of electronic stopping for a certain composition as well as of scattering cross-sections for different atom types, RBS data give information about the depth distribution of atom types.

2.3 Photoluminescence measurements

For photoluminescence (PL) measurements the implanted Er is pumped with an Ar laser. Part of the light emitted by the Er is projected on the entrance slit of a monochromator. Part of the diffraction pattern induced by the grating inside the monochromator is projected onto a germanium detector through the exit slit. Wavelengths are selected by adjusting the orientation of the grating. The experimental setup that was used is shown in figure 3.

To distinguish the low PL signal from detector noise, a lock-in detection technique is used. The Er luminescence signal is modulated with a given frequency. The detected signal is then passed on to the lock-in amplifier. By filtering out all but the selected frequency, the lock-in amplifier drastically increases the signal to noise ratio. The signal modulation is acquired by chopping the pump beam mechanically. To ensure sharp cut-off, the laser beam is focused on the chopper blade. The detected signal is stored on a computer as a function of wavelength.

For measurements of the decay time constant of the 1.5μm level, the detector signal has to be monitored directly. This is done by displaying the bare detector signal on an oscilloscope and registering each decay characteristic with a calibrated camera system attached to the scope. In this case the decay curves are averaged on a computer to improve the signal to noise ratio.

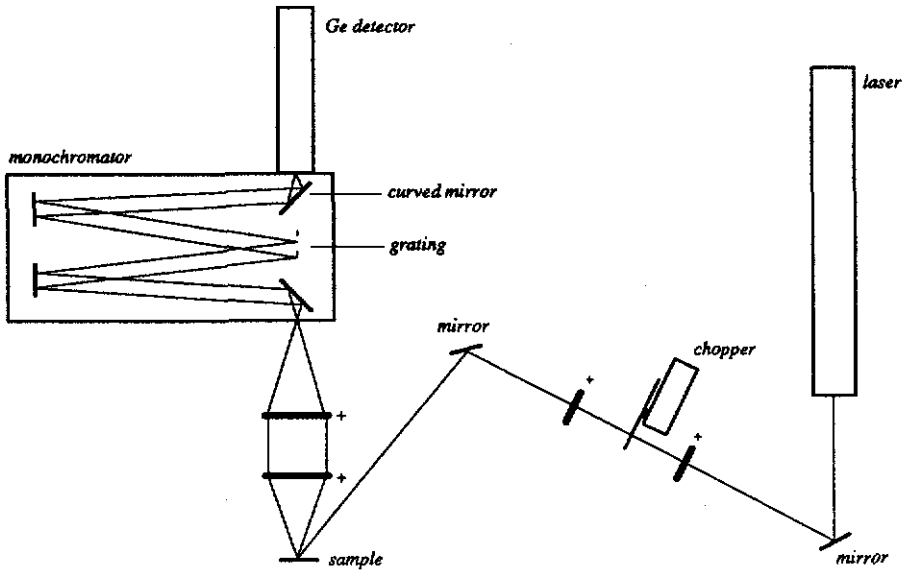

fig 3: Setup for photoluminescence measurements

3. ERBIUM IMPLANTATION IN BGG31 FOR USE IN PLANAR AMPLIFIERS

3.1 Introduction

It has been shown that Er implantation in Fisher soda-lime results in good luminescence characteristics.[5] Fisher soda-lime waveguides, made by the potassium ion exchange process however show poor transmission characteristics,[3] with intensity losses of 0.8 dB/cm. As the net gain in common amplifiers is on the order of 1 dB/cm, this loss is highly significant.

BGG31 glass has been designed especially for the fabrication of low loss optical waveguides by means of the silver ion exchange process.[6] In this glass lower waveguide losses are expected. The composition of BGG31 as found by RBS is shown in table 1. To check if Er implantation in BGG31 could lead to efficient planar light amplifiers, the luminescence behaviour of this system has been investigated.

3.2 Experiment

Five fluences of Er have been implanted in 2 mm thick BGG31 slices, ranging from $9.1 \cdot 10^{14}$ Er/cm^2 to $1.2 \cdot 10^{16}$ Er/cm^2, at an implantation energy of 400 keV and a current density of 2 μA/cm^2. For each of the implants the Er fluence has been determined within five percent using RBS with 2 MeV $^4He^+$ particles. The energy resolution of the detector is 14 keV. For each fluence different samples have been annealed in vacuum (10^{-6} mbar) for one hour. The annealing temperatures ranged from 300°C to 600°C.

Photoluminescence measurements were performed using the 488 nm Ar laser line to excite the Er. Typical pump light intensities were 0.1 kW cm^{-2} in a 1 mm diameter focus. Luminescence spectra were measured using a monochromator with a 600 lines/mm grating and a germanium detector with a sensitive wavelength region ranging from 700 nm up to 1700 nm. Resolutions up to 1 nm were reached for accurate luminescence peak structure measurements. The detector signal was amplified using a lock-in technique. Lifetime measurements were done at the peak wavelength, accepting a spectral width of 6 nm.

Infrared (IR) transmission measurements have been performed in the wavelength region 2.5 μm to 5 μm using a Perkin-Elmer 881 Infrared Spectrophotometer.

Glass component	Weight %
SiO_2	55.0
B_2O_3	10.9
Na_2O	10.9
K_2O	0.023
Al_2O_3	18.7
As_2O_3	0.25
F	4.1
Fe	<0.01

table 1: composition of BGG31 as determined by RBS measurements.

3.3 Results

An RBS measurement of Er implanted BGG31 is shown in figure 4. The lower axis gives the detection channel, which is transformed into an energy scale with the use of a calibration sample. The top axis gives the energy of the backscattered He ions, while the left axis gives a measure for the number of counts in each energy interval. The implanted Er concentration profile has a Gaussian shape with a full width at half maximum (FWHM) of 90 nm and peaks at 120 nm below the surface. The implanted Er fluence is $1.6 \cdot 10^{15}$ Er/cm^2. The peak of the Gauss corresponds to an Er concentration of 0.24 at.%. The sharp peak at 1.1 MeV corresponds to a thin aluminium layer that was deposited on the sample surface to prevent charging of the glass during ion implantation and RBS measurements. Also indicated in the figure are the energies of the helium ions when scattered from a specific element in the sample surface. Due to the stopping process in the Al top layer all elements occur at a slightly lower energy. The solid line is the result of a RUMP simulation with the BGG31 composition from table 1. Apart from the elements shown in table 1, a heavy element with a mass near that of lead was found. Because of the decreasing resolution for higher masses the identity of this element could not be determined.

Figure 5 shows the PL spectrum of a sample containing $9.1 \cdot 10^{14}$ Er/cm^2, annealed at 400°C. The sample shows a broad luminescence spectrum with a FWHM of 50 nm. Maximum luminescence intensity is found at a wavelength of 1532 nm. The observed peak seems to be composed of at least four broad transitions, caused by Stark splitting of the energy levels. At room temperature these peaks could not be resolved. The measured spectra do not show significant differences for different fluences after various annealing treatments.

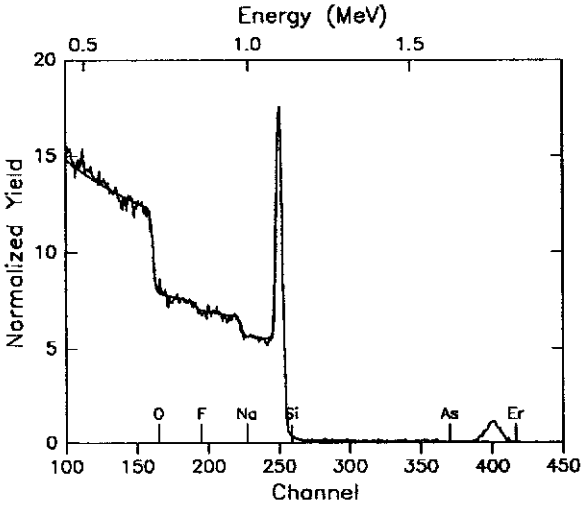

fig 4: RBS spectrum of Er implanted BGG31 at a fluence of $1.6 \cdot 10^{15}$ Er/cm^2. The top axis indicates the energy of the backscattered He^+ ions. The smooth line is a RUMP simulation. The surface channels of several elements are indicated.

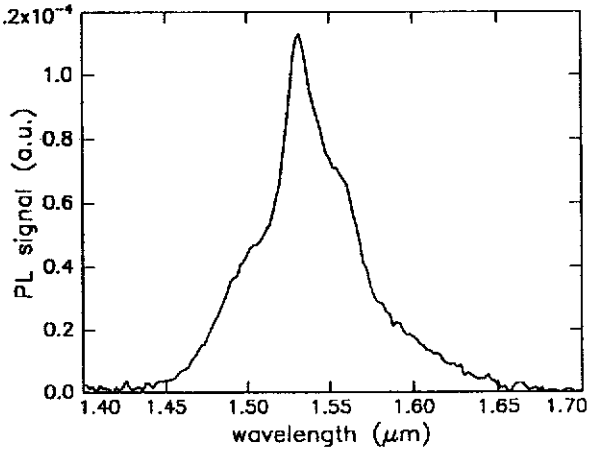

fig 5: Photoluminescence spectrum of Er in BGG31, fluence $9.1 \cdot 10^{14}$ Er/cm^2, annealed for 1 hr at 400°C, 1000 mW 488 nm pump power; resolution 4.8 nm; taken at room temperature.

Figure 6 shows the time dependence of the PL intensity after switching on the pump (fig. 6a) and after the pump is switched off (fig. 6b) for a fluence of $3.0 \cdot 10^{15}$ Er/cm^2, annealed for 1 hr at 500°C. These measurements were performed using high intensity pump light. By focusing the laser beam on the sample surface the intensity was raised to 36 kW cm^{-2} at 1.4 W pump power.

Figure 7 shows the PL peak intensity (solid line) and the decay lifetime (dashed line) as a function of annealing temperature for a fluence of $1.2 \cdot 10^{16}$ Er/cm^2. The figure shows that implantation without an additional annealing treatment yields a low luminescence intensity. Near an annealing temperature of 300°C the intensity starts to increase. The increase levels off for temperatures above 500°C. The decay curves for the samples annealed at temperatures below 350°C were found to be highly non exponential, making it impossible to attribute a single lifetime to these samples. To get a measure for the decay rate, the initial slope of the normalized curves (I=1 for t=0) was measured. The inverse of this value represents an effective lifetime, as will be explained in section 3.4.3. It can be seen that the measure taken for the lifetime exhibits behaviour very similar to that of the intensity.

The intensity measurements were also performed on the other fluences. All showed similar behaviour of the peak intensity. Although the glass transition point lies at 437°C for BGG31, no macroscopic deformation was observed for the samples annealed at 570°C.

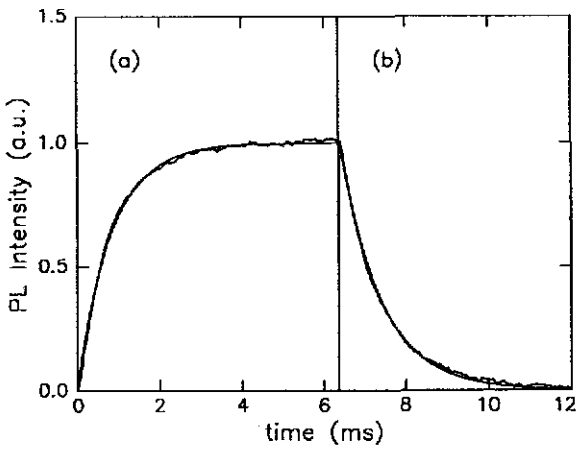

fig 6: averaged PL peak intensity decay after onset of pumping at 36 kW cm^{-2} (a) and after blocking the pump source (b). The Er fluence is $3.0 \cdot 10^{15}$ Er/cm^2, annealed for 1 hr at 500°C. The smooth lines are single exponential fits.

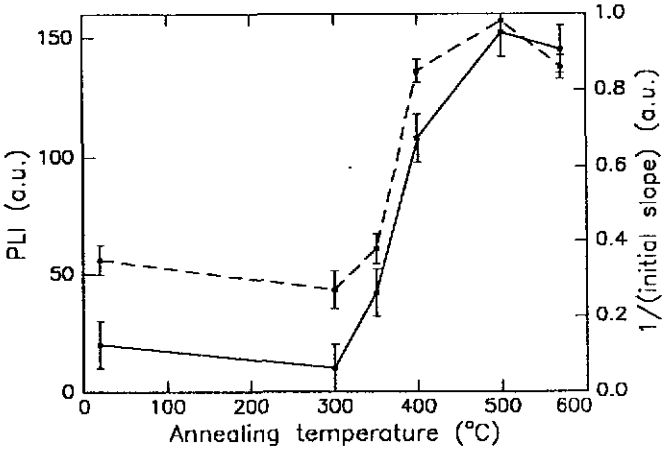

fig 7: PL-Intensity and PL lifetime vs. annealing temperature; fluence $1.6 \cdot 10^{15}$ Er/cm^2; 0.1 kW cm^{-2} pump. The solid line indicates the intensity (left axis) while the dotted line indicates the lifetime (right axis).

In figure 8 the PL peak intensity and the decay lifetime are shown as function of fluence for samples annealed at 400°C for one hour. All samples show perfect exponential signal decay. As can be seen the peak intensity increases with increasing Er fluence. Above a fluence of $3.0 \cdot 10^{15}$ Er/cm^2 the intensity increase becomes sub linear. Simultaneously the decay lifetime decreases as function of fluence.

Figure 9 shows the behaviour of the PL peak intensity as function of pump power for three fluences: $3.0 \cdot 10^{15}$ Er/cm^2, $6.3 \cdot 10^{15}$ Er/cm^2 and $1.2 \cdot 10^{16}$ Er/cm^2, corresponding to peak concentrations of 0.42 at.%, 0.85 at.% and 1.7 at.%. All samples had been annealed at 400°C. The maximum pump power of 1400 mW corresponds to 36 kW cm^{-2}. The curves indicate linear dependence of peak intensity on pump power below 200 mW. For higher pump powers the peak intensity starts to saturate.

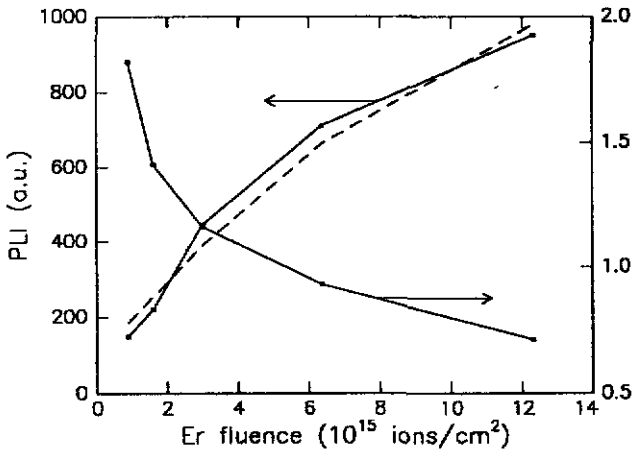

fig 8: PL intensity and PL lifetime versus implanted fluence at 0.1 kW cm^{-2} pump. The dashed line is a calculation described in section 3.4.4.

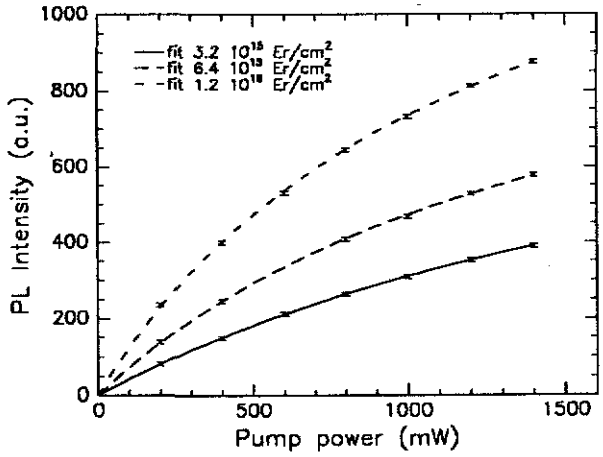

fig 9: PLI versus pump power for three Er fluences annealed at 400°C. The lines are fits through the data points.

The saturation time constant τ_{sat} (fig 6a) and decay lifetime τ (fig 6b) were determined as function of pump power for a fluence of $3.0 \cdot 10^{15}$ Er/cm^2, annealed at 400°C. The power ranges from 400 mW to 1400 mW, corresponding to intensities from 10 kW cm^{-2} to 36 kW cm^{-2}. The inverse values of the measured lifetimes are plotted in figure 10. Both time constants turn out to be of the order of 1 ms at these pump intensities. It can be seen that the decay lifetime remains constant over the whole pump power range. The saturation time constant decreases to 0.78 ms for increasing pump power.

The infrared transmission of unimplanted BGG31 was measured from 2.5μm to 5μm. For comparison the infrared transmission of a 1 mm thick Fisher soda-lime glass slide was also measured. The results are shown in fig 11. The lower axis gives the wavenumber of the infrared radiation, while the top axis gives the corresponding wavelength. Clearly BGG31 shows stronger infrared absorption at 2.8μm and 3.5 μm than Fisher soda-lime glass. Annealing of the glass does not change the transmission characteristics.

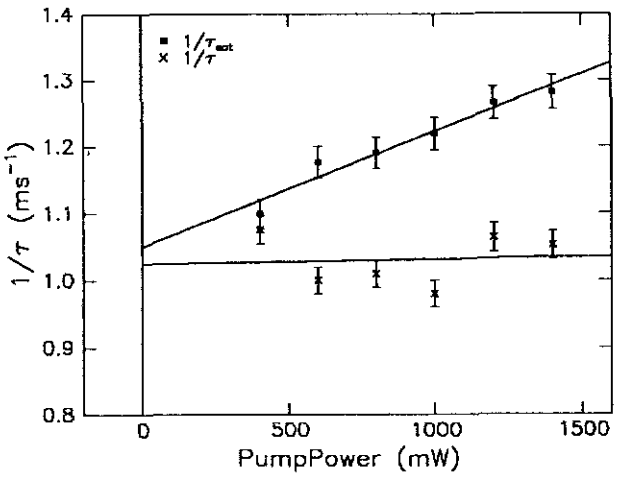

fig 10: Decay lifetime and saturation lifetime versus pump power for an Er fluence of $3.0 \cdot 10^{15}$ Er/cm^2, annealed at 400°C for one hour. The highest pump power corresponds to 18 kW cm^{-2}. The lines are linear fits through the data.

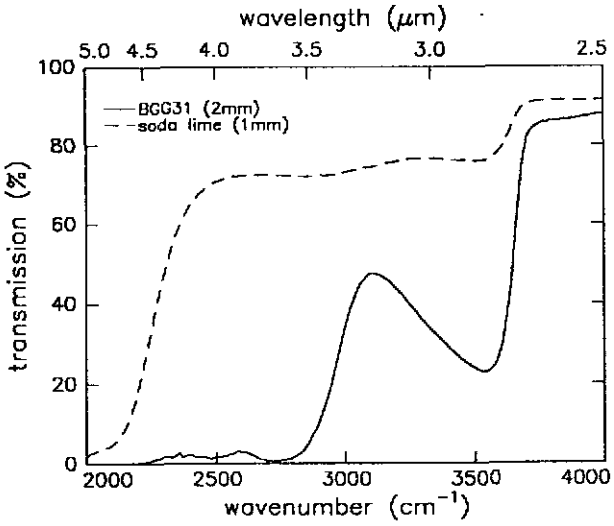

fig 11: IR transmission spectrum for 2 mm thick BGG31 (solid line) and 1 mm thick Fisher soda- lime (dashed line), both unimplanted and unannealed.

3.4 Discussion

3.4.1 Rate equations for the Er^{3+} system

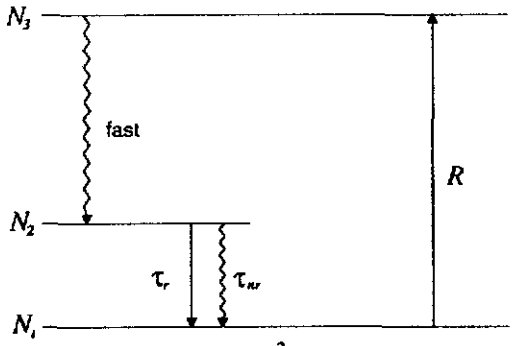

fig 12: The simplified Er^{3+} system.

In the discussion of the results, we will describe the Er^{3+} intra 4f level system as a three level system (fig. 12). The ground state represents the 4f spin configuration with the lowest energy. In steady state 4f the Er ion is continuously pumped into the high level 3 at a rate R. The Er ion then rapidly decays into level 2 by means of a multiphonon relaxation process. From level 2 the ion decays to the ground state either by emission of 1.5μm photons at a rate W_r or by transferring its energy non radiatively to the local surroundings at a rate W_{nr}. When N_2 Er ions are in level 2, the total decay rate is given by

$$W = W_r + W_{nr} = N_2 \cdot \left(\frac{1}{\tau_r} + \frac{1}{\tau_{nr}} \right) = \frac{N_2}{\tau} \qquad \text{(eq. 1)}$$

where τ is the decay lifetime of the 1.5μm level. The radiative decay rate determines the luminescence intensity. From the rate equations for the three level scheme one can easily derive the following equation for the luminescence intensity:

$$I \propto f \cdot N \cdot \frac{R \cdot \tau}{1 + R \cdot \tau} \cdot \left(\frac{1}{\tau_{rad}} \right) \qquad \text{(eq. 2)}$$

Here f is the Er fraction that is in the 3+ state, referred to as the *active fraction*. N is the implanted areal density of Er ions. R is the rate at which Er ions are pumped into the excited state, the *pumping rate*:

$$R = \frac{\sigma_{abs} \cdot I_{pump}}{h \cdot \nu_{pump}} \qquad \text{(eq. 3)}$$

with σ_{abs} the absorption cross-section for the excitation process, I_{pump} the pump intensity at the sample surface and ν_{pump} the frequency of the pump light. The low pump approximation ($R \cdot \tau << 1$) of equation 2 yields the following expression for the photoluminescence intensity:

$$I \propto f \cdot N_t \cdot \frac{\sigma_{abs} \cdot I_{pump}}{h \cdot \nu_{pump}} \cdot \left(\frac{\tau}{\tau_r} \right) \qquad \text{(eq. 4)}$$

3.4.2 The Er^{3+} photoluminescence spectrum

The Er photoluminescence spectrum in BGG31 (fig. 5) shows characteristic $^4I_{13/2} \rightarrow {}^4I_{15/2}$ luminescence.[7] The broadness of the spectrum is to a large degree caused by Stark splitting[7] of the energy levels involved. This Stark splitting results in the underlying peak structure. The broadness of the individual Stark lines is also caused by perturbation of the 4f electron wave functions. The influence of the surrounding glass matrix on the 4f electrons varies as function of time by thermal movement of the matrix, resulting in broadening of the Stark lines of individual ions, and might also differ throughout the material, yielding a broadening caused by a superposition of shifted lines. These two types of broadening are referred to as homogeneous and inhomogeneous broadening. The fact that the observed spectra do not change significantly after the various treatments means that the annealing process does not affect the inner 4f energy levels of most optically active Er ions.

3.4.3 Annealing behaviour of PL Intensity

The photoluminescence lifetime is found to increase as function of annealing temperature (fig. 7). This increase is commonly attributed to removal of implantation induced defects in the glass during annealing. These defects, such as dangling bonds of various kinds, are thought to accept the energy of the excited Er state non radiatively. The removal of defects decreases the non radiative decay rate, and thereby enhances the quantum efficiency of the transition. The decrease of the non radiative decay rate also leads to a longer decay lifetime. As the coupling strength between a defect and the excited erbium depends on distance, different erbium ions are bound to have different decay lifetimes, resulting in a non exponential decay of the PL signal. Indeed for the lower annealing temperatures a strong non exponential behaviour is observed.

As it is not possible to determine a single decay constant for the low annealing temperatures, different rate equations should be used to describe the luminescence intensity as function of annealing temperature. When a range of lifetimes is involved, the measured intensity decay curve is a superposition of a number of decay curves. Each set of ions with identical decay lifetimes τ_i can be pumped up to a certain degree of inversion, with a corresponding luminescence intensity. For each set this determines the initial intensity for the decay curve after blocking the pump light. The total decay curve is thus composed of a number of curves, each with their own initial intensity I_i and their own decay lifetime τ_i. After any annealing treatment the shape of the decay curve can be written as:

$$\frac{I}{I_0} = \frac{\sum_i I_i \cdot e^{-t/\tau_i}}{\sum_i I_i} \qquad \text{(eq. 5)}$$

In the low pump regime (eq. 4) the initial intensities I_i are given by

$$I_i \propto a_i \cdot f \cdot N \cdot R \cdot \frac{\tau_i}{\tau_r} \qquad \text{(eq. 6)}$$

with a_i the fraction of ions in set i and τ_r the radiative lifetime.

Taking the derivative of equation 5 we find the following equation for the initial decrease in intensity:

$$\frac{1}{I_0}\left(\frac{dI}{dt}\right)_{t=0} = \frac{1}{I_0}\left(\sum_i -[I_i]\cdot\frac{1}{\tau_i}e^{-t/\tau_i}\right)_{t=0}$$

$$= \frac{1}{I_0}\left(\sum_i -\left[a_i\cdot f\cdot N\cdot R\cdot\frac{\tau_i}{\tau_r}\right]\cdot\frac{1}{\tau_i}\right) = -f\cdot N\cdot R\cdot\frac{1}{\tau_r}\frac{1}{I_0} \qquad \text{(eq. 7)}$$

where in the last step the active fraction f, τ_r and σ_{abs} are taken to be the same for each set. This means that if the applied model is correct, even in case of non exponential decay the measured intensities should scale with the inverse of the initial decay. In figure 7 the inverse of I_0 is plotted as function of annealing temperature. Good correspondence with the measured intensities is found for the higher annealing temperatures, but for temperatures below 350°C the intensity is lower than expected. This would correspond to either a lower absorption cross-section, a longer radiative lifetime or a lower active fraction for samples annealed below 350°C.

3.4.4 Dose dependence of the PL intensity

In fig 8 it can be seen that the luminescence lifetime decreases with dose while the PL peak intensity increases sub linearly with dose. The dashed in line figure 8 was calculated by multiplying the fluence (N) with the measured lifetimes (τ). The calculated line describes the measured intensities quite well. Comparing with equation 4, this leads to the conclusion that the factor $f\cdot\sigma_{abs}\cdot\tau_r^{-1}$ is constant as function of fluence. This means that the observed sublinearly is due to an increase of the non radiative decay rate, reducing the quantum efficiency of the transition. The observed increase in non radiative decay could be caused by a higher concentration of luminescence quenching centres such as implantation induced defects, for higher fluence. Another possibility is a more efficient coupling to quenching centres at higher fluences due to excited state migration. Migration of excited states to neighbouring erbium ions increases the chance for an excited state to reach a quenching centre, thereby increasing the non radiative decay rate.

3.4.5 PL intensity vs. pump power

For high pump powers, where $R\cdot\tau$ is of the order of 1, equation 2 should be used to explain the obtained intensities. The measured intensities as function of pump power have been fitted with the inversion curve from equation 2, as shown in figure 9. As can be seen this leads to perfect fits for all samples. The fit parameters were the factor $(f\cdot N/\tau_r)$ and the factor (σ_{abs}/S) with $S\approx 4\cdot10^{-5}$ cm^2 the area of the laser spot, shown in table 2. When (f/τ_r) is set to 1 for the lowest fluence, for the higher fluences a lower value is found. This means that the increase in absorption cross-section should be accompanied by an equal decrease in (f/τ_r) to account for the measured intensities. As can be seen the product of the two fitting parameters is quite constant.

Er fluence (cm^{-2})	f/τ_r *fit*	σ_{abs}/S *fit*	$(f/\tau_r)\cdot(\sigma_{abs}/S)$
$3.0\cdot10^{15}$	≡1.0	$1.4\cdot10^{-16}\pm2\%$	$1.4\cdot10^{-16}$
$6.3\cdot10^{15}$	$0.55\pm5\%$	$2.5\cdot10^{-16}\pm4\%$	$1.4\cdot10^{-16}$
$1.2\cdot10^{16}$	$0.37\pm5\%$	$4.5\cdot10^{-16}\pm3\%$	$1.7\cdot10^{-16}$

table 2: absorption cross sections and active fractions as found by fitting the PL intensity vs. pump power curves.

These results are in accordance with the conclusion of paragraph 3.4.4, in which was shown that for these samples the factor $f \cdot \sigma_{abs} \cdot \tau_r^{-1}$ is constant for low pump intensity. This turns out to be the case over the whole range of pump intensities.

The strong variation of the absorption cross-section may be explained by shifts in the absorption bands around 500 nm for different fluences. As the absorption bands are very sharp,[4] a shift relative to the pump wavelength could result in strong variations in absorption cross-section. The fitted decrease in the factor $f \cdot \tau_r^{-1}$ could indicate that at higher Er fluences not all Er can be activated.

An alternative explanation for the differences in fitted absorption cross-section could be that efficiency decreasing effects are gradually starting to play a role for high degrees of inversion, resulting in a stronger curvature of the lines in figure 9. These effects might include for example upconversion,[8] in which due to interaction between two excited Er ions, effectively one excited state is lost. Any explanation however should account for the fact that the effects lead to perfect inversion curves as shown in figure 9. If such effects indeed influence the fitted cross-sections, then the values in table 2 should be considered an upper limit for the absorption cross-section at 488 nm.

To derive a value for the absorption cross-section, the laser spot size was determined. This was done by scanning a thin metal wire through the focus while measuring the amount of diffusely scattered light from the wire with the monochromator. The spot width at 1/e intensity was 0.07 mm ± 0.02 mm, yielding an upper limit of $\sigma_{abs} = 5.4 \cdot 10^{-21}\,\mathrm{cm}^2 \pm 30\%$.

3.4.6 Saturation characteristics

The time dependent behaviour of the photoluminescence intensity also gives information about the absorption cross-section. By writing down the rate equations for the three level system and solving the resulting differential equation we find the following equation for the photoluminescence intensity:

$$I \propto \frac{f \cdot N}{1 + R \cdot \tau} \cdot \left(1 - \exp\left(-\frac{t}{\tau_{sat}}\right)\right) \qquad \text{(eq. 8)}$$

given a constant pump power and initial luminescence intensity of zero. Here the saturation time constant τ_{sat} is given by

$$\frac{1}{\tau_{sat}} = \left(R + \frac{1}{\tau}\right) \qquad \text{(eq. 9)}$$

This means that after switching on the pump light, the PL intensity approaches its steady state value single-exponentially, with an exponent that contains the absorption cross-section (see eq. 3). The measured intensity increase after switching on the pump at the highest intensity is plotted in figure 6, which shows that the increase is indeed roughly exponential.

The obtained inverted saturation- and decay time constants for the $3.0 \cdot 10^{15}$ Er/cm^2 sample have been fitted linearly as shown in figure 10. It can be seen that the intersection at zero pump power of the two fits as predicted by equation 9 occurs within the experimental error. Determining the slope of the saturation time curve gives a second measurement of the factor (σ_{abs}/S), yielding $0.67 \cdot 10^{-16}$. Again using the measured spot size (section 3.4.5) this gives $\sigma_{abs} = 2.6 \cdot 10^{-21}\,\mathrm{cm}^2 \pm 30\%$. This is significantly lower than the value of $5.4 \cdot 10^{-21}\,\mathrm{cm}^2 \pm 30\%$ as found by fitting the inversion curves for the same sample (section 3.4.5). This makes it likely that already for this fluence high order effects such as upconversion play a role, so that the values for the absorption cross-sections from table 2 should indeed be considered upper

limits. As high order effects would alter the decay rate τ^{-1} during the rise to higher inversion, it is clear that this would alter the exponential signal increase as predicted by equation 8. A closer look at figure 6 shows that the signal increase is not completely exponential at higher intensity. This gives further evidence for the presence of high order effects such as upconversion. As it is not clear in what way this affects the fitted saturation times, the upper limit for the absorption cross-section is taken to be $5.4 \cdot 10^{-21}$ $cm^2 \pm 30\%$ as found in section 3.4.5.

3.4.7 Infrared absorption measurements

The decay lifetimes as found in BGG31 are very low compared to those found for similar Er fluences in Fisher soda-lime glass, where lifetimes of the order of 10 ms have been observed.[5] Apparently in BGG31 the luminescence is quenched strongly. Hydroxide groups have been suggested as luminescence quenching centre in the 1.5μm regime, because of their vibration stretch band at a wavelength of 3 μm. The second order harmonic of this vibration coincides with the Er luminescence wavelength, and is believed to couple non radiatively to the excited state.

The infrared-transmission spectrum for both glasses is shown in figure 11. The absorption dip at 2.8 μm gives a measure of the OH content. Although it should be noted that the samples have different thicknesses, it is clear that at this wavelength BGG31 shows stronger infrared absorption than Fisher soda-lime glass. The presence of OH thus could account for the low lifetimes found in BGG31. This conclusion is supported by measurements described in the next chapter, in which again the measured lifetimes are correlated to the infrared absorption.

3.5 Conclusions

Erbium was implanted at 400 keV at fluences from $0.9 \cdot 10^{15}$ Er/cm^2 to $1.2 \cdot 10^{16}$ Er/cm^2 into BGG31, a silica glass designed for the fabrication of ion exchanged waveguides. Annealing up to 570°C increases the Er photoluminescence intensity due to a decrease in non radiative interaction with luminescence quenching centres, possibly in combination with an increase in the fraction of optically active Er. The photoluminescence intensity is found to increase sublinearly with Er fluence. This behaviour is described by a decrease in the lifetime for higher fluences, attributed to Er-Er interactions and Er-defect interactions at high concentrations. The data suggest that after annealing the active fraction as well as the absorption cross-section and radiative lifetime are the same for all annealed Er fluences.

The photoluminescence lifetimes were of the order of 1 ms. The fact that the lifetimes are low compared to those found for Er implanted in Fisher soda-lime glass could be caused by the presence of luminescence quenching OH groups in the glass as identified by IR spectroscopy.

Two independent ways of measuring the absorption cross-section at high pump power, based on a three level model for the Er^{3+} level system, arrived at different values for the same Er fluence. This leads to the conclusion that in BGG31 at high pump powers other processes than those included in the three level model play a role. These effects might include upconversion. An upper limit for the absorption cross-section at 488 nm was determined, yielding $\sigma_{abs} = 5.4 \cdot 10^{-21} cm^2 \pm 30\%$.

4. ERBIUM LUMINESCENCE LIFETIMES IN OTHER GLASS HOSTS

4.1 Introduction

In BGG31 glass a low photoluminescence lifetime is found, making this material less attractive as amplifying medium. The low lifetime may be caused by the presence of OH groups, which are thought to couple non radiatively to the Er excited state. In addition to the experiments described in chapter 3 four other commercially available sodium containing glasses have been examined briefly, as an outlook for future experiments on waveguides. A clear correlation between OH concentration and photoluminescence lifetime is found.

4.2 Experiment

Erbium was implanted at 500 keV into Pilkington soda-lime glass (PSL), witglas (WG), Tempax (TPX) and in Corning 0211 glass (CRN) at a current density of 0.7 $\mu A/cm^2$. The implanted fluences were determined within five percent using RBS (table 3). The experimental conditions were equal to those in the experiments on BGG31, unless separately specified.

Anneals were performed in-vacuum (10^{-6} mbar) for one hour at temperatures ranging from 300°C to 600°C. On all glasses photoluminescence (PL) measurements were performed, again using the 488 nm Ar line as excitation source. Lifetime measurements were done at the peak wavelength, accepting a spectral width of roughly 25 nm.

Infrared (IR) transmission measurements as well as infrared reflection measurements have been performed on all glasses in the wavelength region 2.5 μm to 5 μm using a Perkin-Elmer 881 Infrared Spectrophotometer.

Glass type	thickness (mm)	Er fluence (Er/cm^2)
Pilkington soda-lime (PSL)	0.65	$1.7 \cdot 10^{15}$
Corning 0211 (CRN)	0.60	$1.9 \cdot 10^{15}$
Tempax (TPX)	1.85	$1.9 \cdot 10^{15}$
Witglas (WG)	0.90	$1.7 \cdot 10^{15}$

table 3: implanted fluences as determined by RBS and sample thickness.

4.3 Results

The measured RBS spectra are shown in the appendix (fig. 14, 17, 20 and 23). In each spectrum the top axis indicates the energy of the backscattered particles, calculated from the detection channel (lower axis) with the use of a calibration sample. The left axis gives a measure for the number of backscattered particles in each energy interval. The RBS data were analysed using the RUMP simulation program. The smooth lines in the spectra represent the RUMP simulations as found after inserting the compositions from table 4. The sharp peak for the PSL, WG and CRN samples near channel 250 is due to an aluminium layer that had been deposited on the samples to prevent charging of the samples during implantation and RBS measurements. For the CRN sample the composition was specified by the manufacturer, leading to a good fit (fig 23). An additional heavy element near an atomic weight of 128 is observed in the unimplanted CRN samples. For the other glasses the composition as shown in table 4 is a rough approximation within the limits of RBS. Due to the small mass difference between Ca and K, these two elements could not be distinguished with RBS. As Ca is a well known ingredient for soda-lime however, the bump at channel 300 in the Pilkington soda-lime is probably due to Ca.

The PL spectra for all glasses are also shown in the appendix (fig. 15, 18, 21 and 24). All show clear Er^{3+} luminescence, with features similar to those found in BGG31 (section 3.4.3). For the annealed TPX sample the individual Stark lines are much broader than in the other glasses. All samples show significant changes in spectrum for different annealing treatments. The peak intensities however remain in place. The position of the peak intensities as well as the FWHM of the spectra are shown in table 5.

The PL peak intensity was measured as function of annealing temperature, as shown in the appendix. This peak intensity does *not* represent the integrated intensity, as the PL spectra show different shapes for different annealing treatments. In the CRN sample the PL intensity starts to increase near 400°C, while for the other glasses this increase occurs near 300°C. For the WG and CRN samples the intensity does not show saturation. The PSL sample seems to saturate near 600°C. The intensity decrease as found in the TPX sample has not yet been verified.

For all samples the PL decay characteristics were measured for different annealing temperatures. All show non exponential decay for the low annealing temperatures, while for higher temperatures the decay is nearly exponential. For the exponential curves, the decay lifetime was determined as shown in table 6. Although the TPX decay curve for a 500°C anneal is non exponential, the average decay lifetime seems to be of the order of 1.5 ms, which is longer than the lifetime of 0.9 ms found after a 600°C anneal.

The IR transmission measurements yielded the *total* IR transmission. By evaluating IR reflection measurements (not shown) it was found that for all samples the IR transmission was decreased by 7±2% due to specular reflection at the interfaces. The transmission data were corrected for 7% reflection,

element	mass	CRN	WG	PSL	TPX
Si	28.1	21.4	24.6	25.0	28.0
Na	23.0	5.5	6.5	11.5	3.0
K/Ca	39/40	2.7/0	7	3	?
O	16.0	61.6	60.1	60.3	69.0
Al	27.0	1.6	-	-	-
B	10.8	4.6	-	-	-
Ti	47.9	0.8	<0.4	-	-
Zn	65.4	1.75	1.0	-	-
?	133±5	-	0.32	-	-
?	128±7	<0.05	-	-	-

table 4: compositions in at.% as found by RBS (columns 4-6) and from literature (column 3)

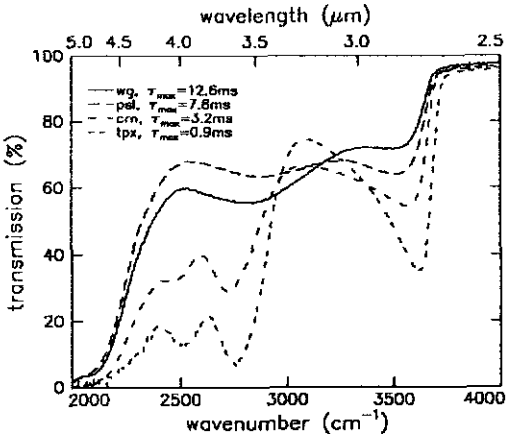

figure 13: infrared transmission per mm for Witglas, Pilkington soda-lime, Corning 0211 and Tempax. The lifetime found for these samples is also indicated.

introducing an error of 2%. Assuming homogeneous sample composition the corrected values for the transmission were scaled to transmission per millimeter. The results of these calculations are shown in figure 13.

4.4 Discussion

All photoluminescence spectra show characteristic Er^{3+} luminescence. The general characteristics of these spectra have been discussed in section 3.4.2. The broadness of the Tempax spectrum probably reflect stronger interaction between the Er intra 4f states and the surrounding material.

The depth of the absorption dip in fig. 13 near 3 μm is related to the amount of OH in the glass. This group is thought to accept the energy of the excited 1.5 μm state in Er by a non radiative interaction, so that a correlation between OH content and decay lifetimes is expected. A comparison of table 6 with figure 13 shows that this correlation is very clear for the examined glasses. This leads to the important conclusion that for the fabrication of efficient planar Er based amplifiers the OH content of the host material should be kept as low as possible.

It can be seen that low photoluminescence lifetimes are also accompanied by broad photoluminescence spectra. The annealed TPX and BGG31 samples both show a FWHM of the order of 45 nm, and exhibit PL decay lifetimes of the order of 1 ms. The PSL and WG samples show a FWHM of the order of 20 nm, accompanied by PL decay lifetimes of the order of 10 ms. It is not yet clear if the observed broadness of the PL spectra is independent of the OH concentration.

	WG	PSL	CRN	TPX
FWHM (nm)	20	20	24	45
peak pos. (nm)	1532	1537	1537	1533

table 5: Full width half maximum and peak position of the PL spectra of WG, PSL, CRN and TPX after annealing at 600°C for one hour

T_{anneal} (°C)	WG	PSL	CRN	TPX
500	10.2	7.8	non exp.	non exp.
600	12.6	7.4	3.2	0.9

table 6: measured photoluminescence lifetimes (ms).

APPENDIX

Pilkington soda-lime glass

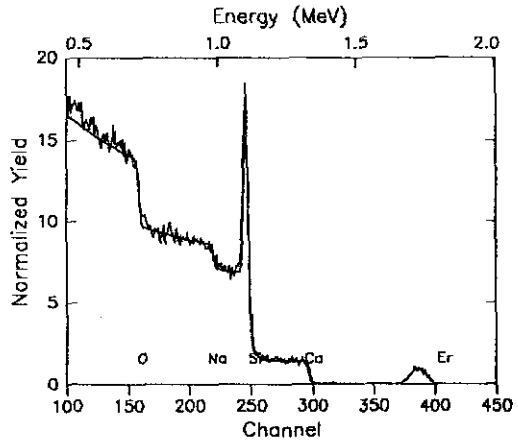

fig 14: RBS spectrum of Pilkington soda-lime glass. The smooth line represents an RBS simulation of the composition shown in table 4. The surface channels of several elements are indicated.

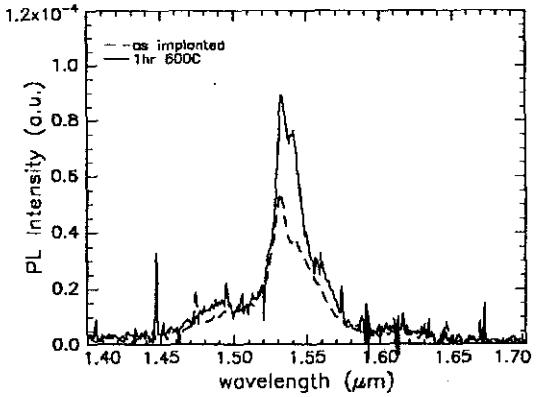

fig 15: PL spectrum of Er implanted in Pilkington soda-lime glass without annealing (dashed line) and after annealing at 600°C for one hour (solid line). Both resolutions 3 nm, pumped at 0.5 kW cm^{-2}

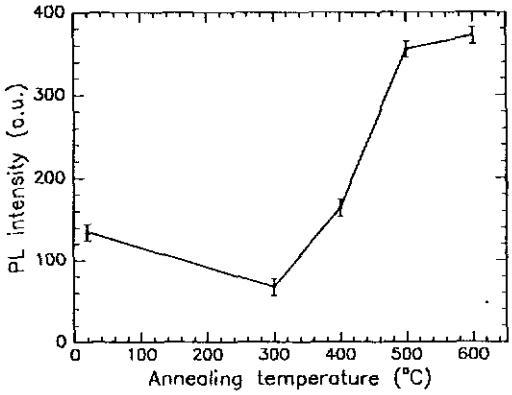

fig 16: PL peak intensities at 1537 nm in Pilkington soda-lime glass after on hour anneals at different temperatures.

Tempax glass

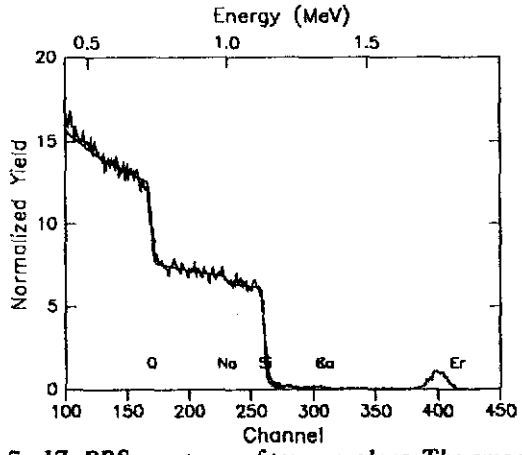

fig 17: RBS spectrum of tempax glass. The smooth line represents an RBS simulation of the composition shown in table 4. The surface channels of several elements are indicated.

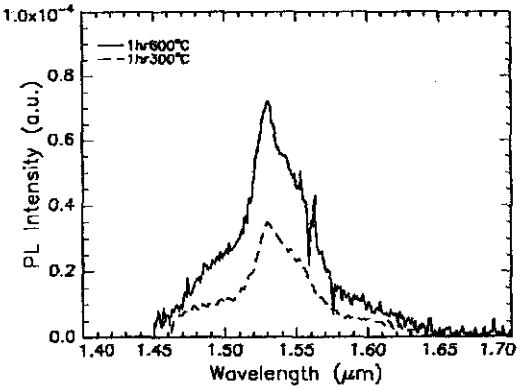

fig 18: PL spectrum of Er implanted in tempax glass after annealing at 300°C for one hour, resolution 6 nm (dashed line) and after annealing at 600°C for one hour, resolution 3 nm(solid line). Both pumped at 0.5 kW cm^{-2}

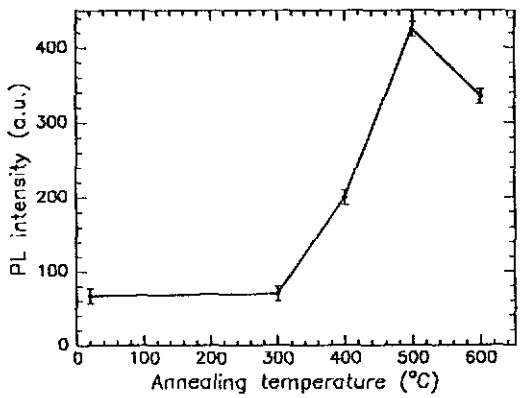

fig 19: PL peak intensities at 1533 nm in tempax glass after on hour anneals at different temperatures.

Witglas

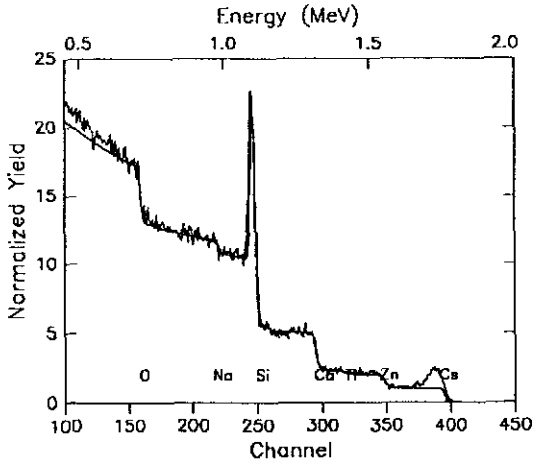

fig 20: RBS spectrum of witglas. The smooth line represents an RBS simulation of the composition shown in table 4. The surface channels of several elements are indicated.

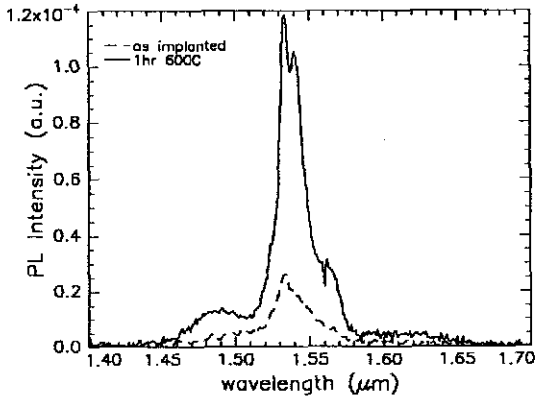

fig 21: PL spectrum of Er implanted in witglas without annealing (dashed line) and after annealing at 600°C for one hour (solid line). Both pumped at 0.25 kW cm^{-2}, resolution 3 nm.

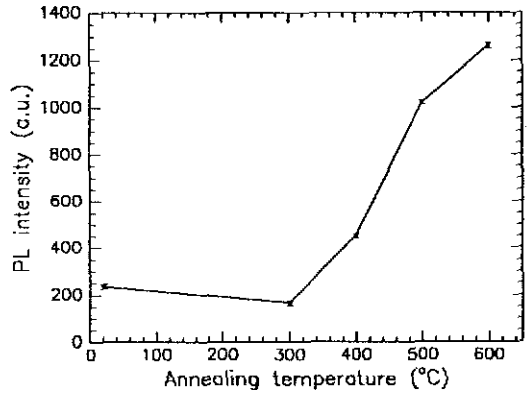

fig 22: PL peak intensities at 1532 nm in witglas after on hour anneals at different temperatures.

Corning 0211 glass

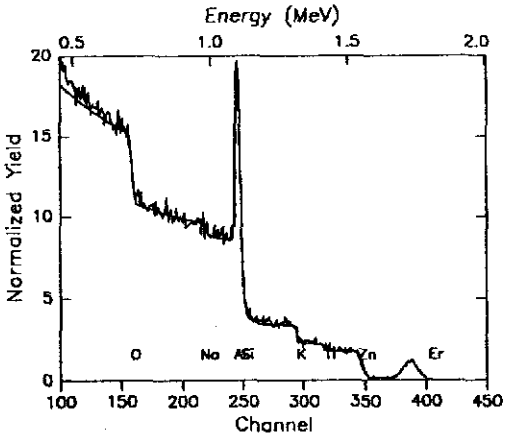

fig 23: RBS spectrum of Corning 0211 glass. The smooth line represents an RBS simulation of the composition shown in table 4. The surface channels of several elements are indicated.

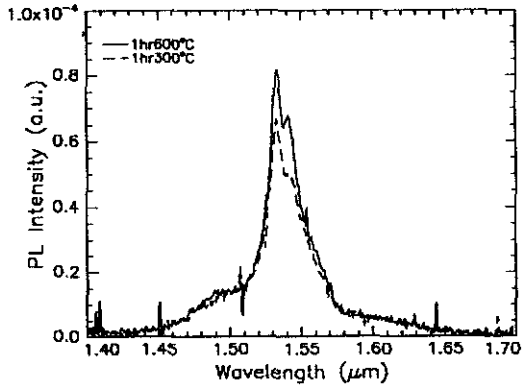

fig 24: PL spectrum of Er implanted in Corning 0211 glass after annealing at 300°C for one hour, pumped at 0.5 kW cm^{-2} (dashed line) and after annealing at 600°C for one hour, pumped at 0.25 kW cm^{-2} (solid line). Both resolutions 3 nm.

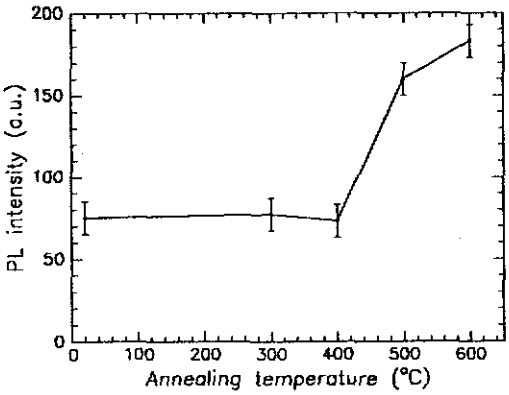

fig 25: PL peak intensities at 1537 nm in Corning 0211 glass after on hour anneals at different temperatures.

References

[1] E. Desurvire: *The golden age of optical fiber amplifiers*, Phys. Today Jan. 1994
[2] J. Shmulovich et al: *15dB net gain demonstration in Er3+ glass waveguide amplifier on silicon*, OSA Optical Amplifier Meeting Feb. 1993
[3] E. Snoeks, G.N. van den Hoven and A Polman, *Doping fibre compatible ion-exchanged channel waveguides with erbium by ion implantation*, Proc. ECIO 1993 p. 3-38, Neuchatel, Switzerland.
[4] W. J. Miniscalco, *Erbium-doped glasses for fiber amplifiers at 1500 nm*, J. Lightw. Tech. **9** (1991)
[5] E.Snoeks, G.N. van den Hoven and A. Polman, *Optical doping of soda-lime-silicate glass with erbium by ion implantation*, J. Appl. Phys. **73**, 8179 (1993)
[6] L. Roß, *Integrated optical components in substrate glasses*, Glastech. Ber. **62** (1989)
[7] S.Hüfner, *Optical spectra of transparent rare earth compounds* (Academic, New York, 1978)
[8] J.C. Wright, in *Radiationless processes in molecules and condensed phases*, F.K. Kong edt., ch. 4. (Springer-Verlag, Heidelberg, 1976).